Supporting Information

For

Synthesis of copolymer derived from tamarind kernel polysaccharide (TKP) and *poly* (methacrylic acid) *via* SI-ATRP with enhanced pH triggered dye removal

Aniruddha Pal, Sagar Pal[*]

Polymer Chemistry Laboratory, Department of Applied Chemistry, Indian School of Mines, Dhanbad-826004, India

19 February 2018

Note added after first publication: This Supplementary Information file replaces that originally published on 22 December 2015, in which an incorrect image was included in Fig. S5.

* Corresponding Author: Tel: +91-326-2235769; Fax: 0091-326-2296615

E-mail: sagarpal1@hotmail.com

AFM analysis:

Sectional analysis and the roughness measurements were performed over the entire scan size of 10μm×10μm, using AFM instrument (Bruker Dimension Icon Nanoscope V, Germany). The root mean square (*r.m.s*) roughness represents the standard deviation of the heights in the topographical image and was calculated using eq. (1)

$$\boldsymbol{r.m.s\ roughness} = \sqrt{\frac{\mathbf{1}}{\boldsymbol{n-1}}\sum_{\boldsymbol{sectional}}(\boldsymbol{Z_i - Z_{average}})^{\mathbf{2}}} \quad \ldots\ldots\ldots\ldots\ldots\ldots\ldots\ldots\ldots\ldots \boldsymbol{eq.}\,(\mathbf{1})$$

Where Z_i is the height value at the *i* point in the image, *n* is the number of points in the image and $Z_{average}$ is the average height calculated by eq. (2)

$$\boldsymbol{Z_{average}} = \frac{\mathbf{1}}{\boldsymbol{n}}\sum_{\boldsymbol{Sectional}}\boldsymbol{Z_i} \quad \ldots\ldots\ldots\ldots\ldots\ldots\ldots\ldots\ldots\ldots\ldots\ldots\ldots \boldsymbol{eq}\,(\mathbf{2})$$

Investigation of rheological characteristics:

The rheological characteristics were examined in the laboratory using Bohlin Gemini-2 Rheometer (Malvern, UK). The system temperature was controlled at 30 ºC throughout the experiments. The aqueous solutions of 1-wt % TKP and various grades of g-TKP/pMA were prepared using pH 7.4 buffer solution. The storage modulas (G') and loss modulas (G") were measured at a constant frequency of 0.25 Hz and different shear stress ranging from 0 to 500 Pa. Frequency sweep measurements were carried out in the frequency range from 0.1 to 10 Hz at a constant stress of 1 Pa. Similarly, Shear viscosity was evaluated at different shear rates regions.

Adsorption Experiments:

In the present study 1000 mg. L-1 stock solutions of different dyes (MB, Safranin, EBT and MO) were prepared individually. Thermostated orbital shaker (Rivotek, Kolkata, India) was used to perform the batch experiments. The experimental parameters such as solution pH, initial

concentration of dyes, contact time, agitation speed, adsorbent dose and temperature were varied to optimize the adsorption condition.

In all batch experiments, required amount of adsorbent was mixed with 25mL of the dye solutions and then the flasks were shaken for desired time at particular temperature. After the filtration, (with the help of 0.42 μm filter paper), the concentration of the dye solutions were analyzed by UV-Vis spectrophotometer (Make: Shimadzu, Japan: Model: UV 1800).

The % of adsorption as well as equilibrium uptake was determined using eq. (3) and eq. (4) respectively

$$Adsorption = \frac{C_0 - C_e}{C_0} \times 100 \ldots\ldots\ldots\ldots\ldots\ldots\ldots\ldots\ldots eq.(3)$$

$$q_e = (C_0 - C_e) \times \frac{V}{W} \ldots\ldots\ldots\ldots\ldots\ldots\ldots\ldots\ldots eq.(4)$$

Where $q_e$is the equilibrium capacity of dyes on adsorbent (mg. g^{-1}), C_0 and C_e are the initial and equilibrium concentration of the dyes (mg L^{-1}), respectively. V is the volume of dye solution used (L) and W is the weight of the adsorbent (g) utilized.

Desorption experiments:

To determine the reusability of g-TKP/pMA as adsorbent, three successive adsorption-desorption experiments were carried out with 400 mg.L^{-1} of MB, 300 mg, L^{-1} of Safranin, 350 mg, L^{-1} of EBT and 300 mg, L^{-1} of MO dye solutions. The dye loaded samples were separated by filtration and the samples were dried completely and used for desorption study. To determine the reusability of the sorbents, consecutive adsorption-desorption cycles were repeated three times with pH 2, 7 and 9.

The % desorption was calculated eq. (5):

$$\%\, Desorption = \frac{Concentration\ desorbed\ (mg/L)}{Concentration\ adsorbed\ (mg/L)} \times 100 - - - - - \ eq.(5)$$

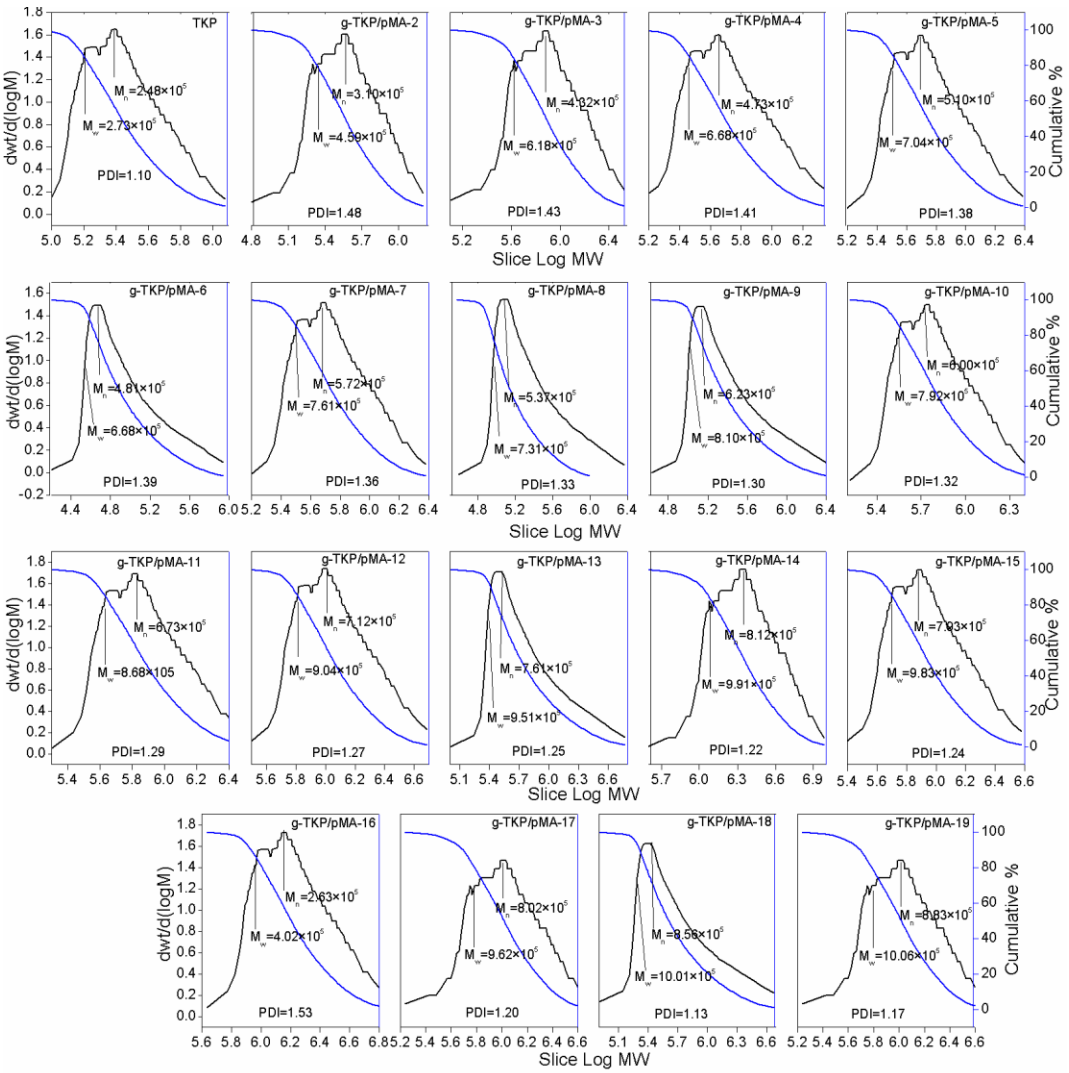

Fig. S1: GPC analysis result

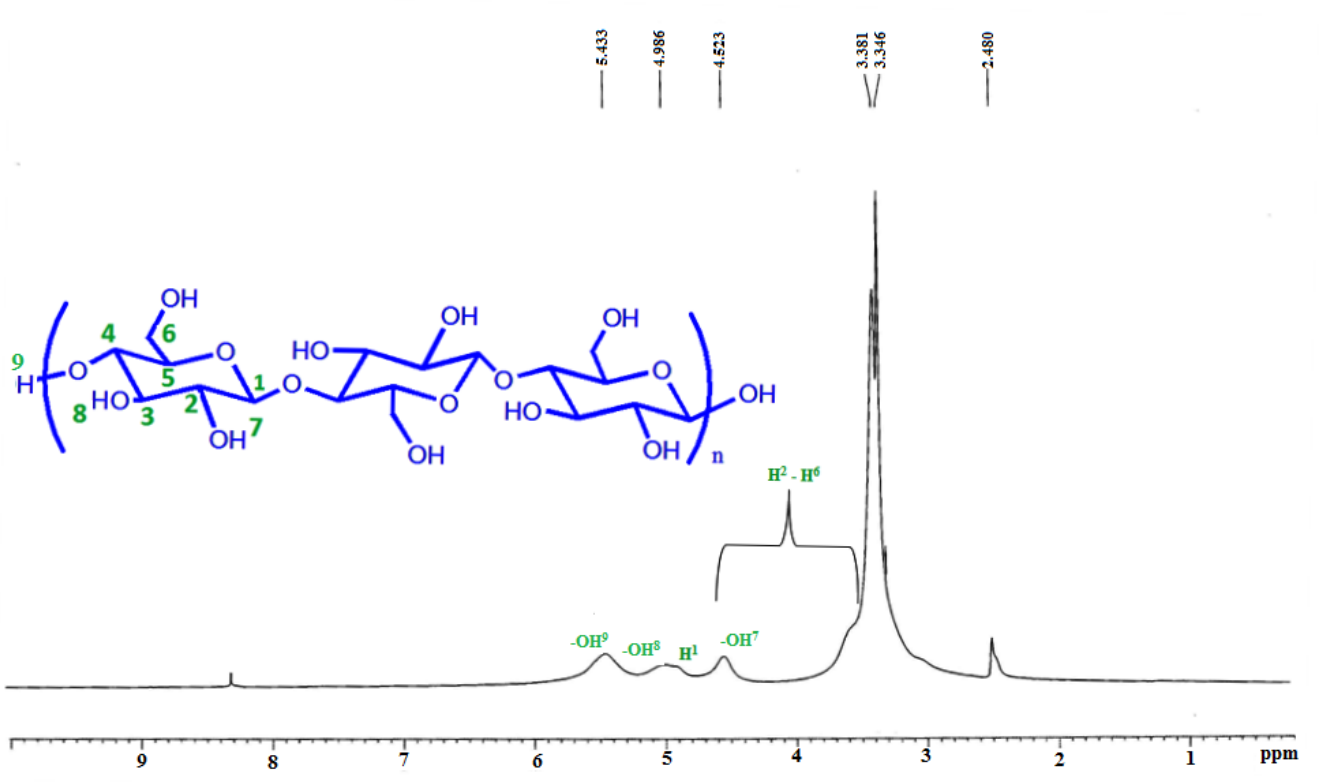

Fig. S2: ^{1}H NMR spectrum of TKP

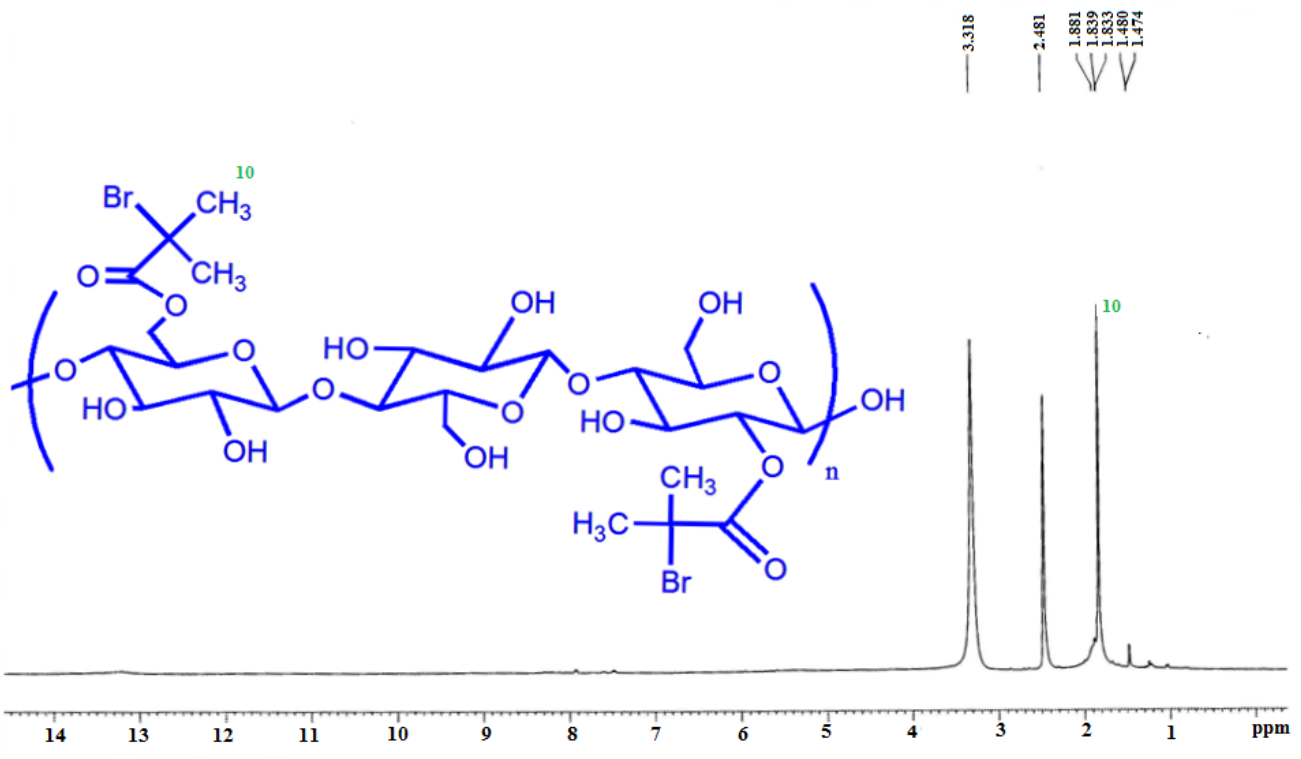

Fig. S3: ^{1}H NMR spectrum of TKP-Br

Table S1. Elemental analysis results

Sample	% C	% H	% N	% O	% S
TKP	40.03	7.42	0.41	52.1	0.00
g-TKP/pMA-18	35.16	6.12	0.14	58.5	0.00

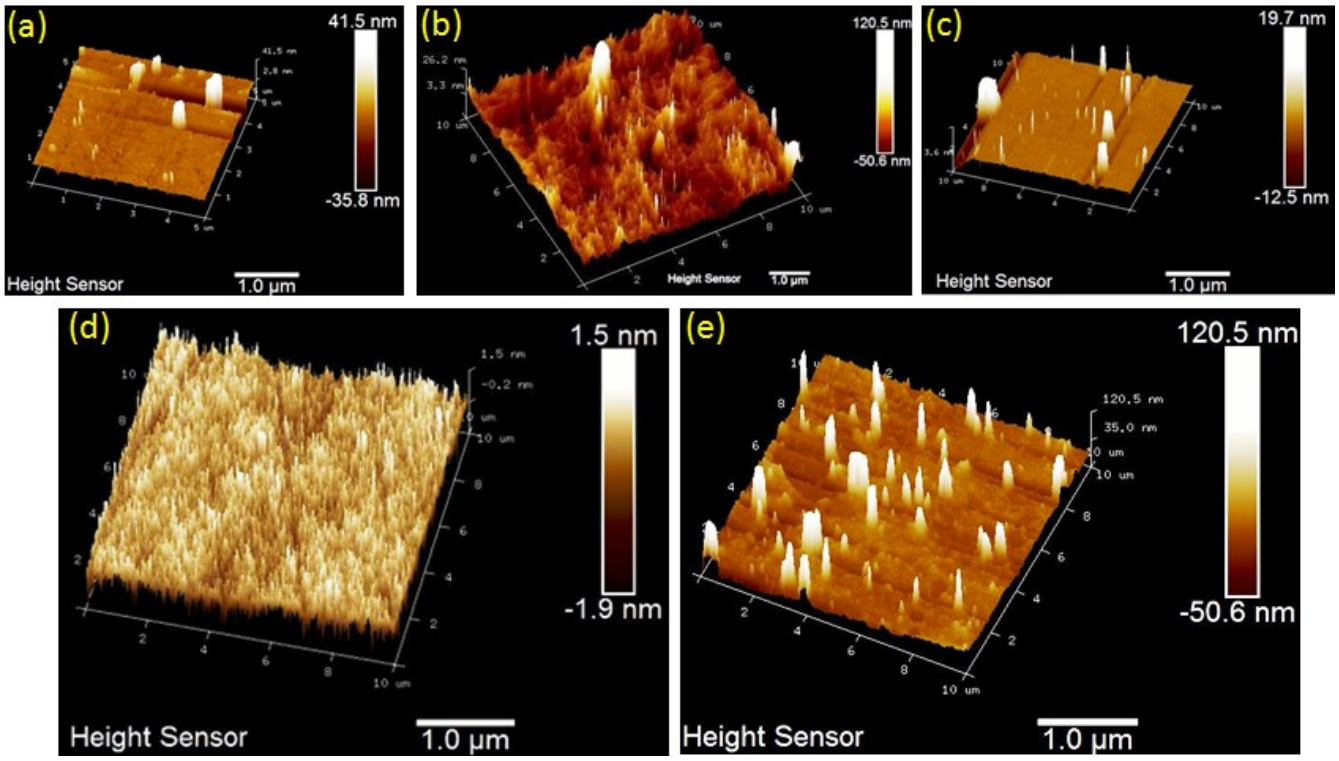

Fig. S4: AFM analysis of (a) TKP (b) TKP-Br (c) g-TKP/pMA (d) MB loaded g-TKP/pMA and (e) EBT loaded g-TKP/pMA

Table S2. Sectional analysis of (a) TKP (b) TKP-Br (c) g-TKP/pMA and (d) MB loaded g-TKP/pMA (e) EBT loaded g-TKP/pMA

(a)

Pair	Horizontal Distance	Vertical Distance	Surface Distance	Angle	Rmax	Rz	Rz Count	Rms	Ra (Freq. Cut Off)	Freq. Cut Off	Radius	Radius Sigma
1	0.67µm	-1.467nm	0.069µm	-1.163(°)	1.749nm	0.000nm	0.000	6.645nm	0.517nm	6.645µm	2.900µm	0.000nm
0	0.000µm	0.000nm	0.000µm	0.000(°)	0.000nm	0.000nm	0.000	0.000nm	0.000nm	0.000µm	0.000µm	0.000nm
0	0.000µm	0.000nm	0.000µm	0.000(°)	0.000nm	0.000nm	0.000	0.000nm	0.000nm	0.000µm	0.000µm	0.000nm

(b)

Pair	Horizontal Distance	Vertical Distance	Surface Distance	Angle	Rmax	Rz	Rz Count	Rms	Ra (Freq. Cut Off)	Frequency Cut Off	Radius	Radius Sigma
1	0.265µm	13.303nm	0.019µm	2.073(°)	34.214.nm	0.000nm	0.000	57.325nm	52.075nm	0.000µm	0.492µm	0.006nm
2	0.112µm	69.206nm	0.146µm	35.23(°)	61.017nm	0.000nm	0.000	5.957nm	45.563nm	0.000µm	0.158µm	0.009nm
3	0.378µm	-4.368nm	0.208µm	-0.401(°)	59.445nm	43.424nm	1.900	0.000nm	18.747nm	0.000µm	0.346µm	0.002nm

(c)

Pair	Horizontal Distance	Vertical Distance	Surface Distance	Angle	Rmax	Rz	Rz Count	Rms	Ra (Freq. Cut Off)	Frequency Cut Off	Radius	Radius Sigma
1	1.440µm	-2.035nm	1.176µm	-0.075(°)	81.386.nm	85.541nm	1.780	41.413nm	29.074nm	0.000µm	2.279µm	0.011nm
2	0.569µm	74.720nm	0.667µm	6.176(°)	72.652nm	0.000nm	0.000	3.777nm	22.472nm	0.000µm	2.034µm	0.002nm
0	0.000µm	0.000nm	0.000µm	0.000(°)	0.000nm	0.000nm	1.070	0.000nm	0.000nm	0.000µm	0.000µm	0.000nm

(d)

Pair	Horizontal Distance	Vertical Distance	Surface Distance	Angle	Rmax	Rz	Rz Count	Rms	Ra (Freq. Cut Off)	Freq. Cut Off	Radius	Radius Sigma
1	1.123µm	2.987nm	1.252µm	0.126(°)	123.88.nm	129.88nm	1.098	46.700nm	42.700nm	0.000µm	1.275µm	0.013nm
2	0.169µm	121.57nm	0.218µm	29.65(°)	72.942nm	0.000nm	0.000	6.089nm	5.089nm	0.728µm	0.256µm	0.051nm
0	0.000µm	0.000nm	0.000µm	0.000(°)	0.000nm	0.000nm	2.120	0.000nm	0.000nm	0.000µm	0.000µm	0.000nm

(e)

Pair	Horizontal Distance	Vertical Distance	Surface Distance	Angle	Rmax	Rz	Rz Count	Rms	Ra (Freq. Cut Off)	Freq. Cut Off	Radius	Radius Sigma
1	1.113µm	2.787nm	1.552µm	0.126(°)	126.84.nm	139.88nm	1.196	49.524nm	45.700nm	0.000µm	1.295µm	0.014nm
2	0.159µm	111.27nm	0.248µm	31.65(°)	72.742nm	0.000nm	0.000	6.129nm	5.119nm	0.788µm	0.266µm	0.061nm
0	0.000µm	0.000nm	0.000µm	0.000(°)	0.000nm	0.000nm	2.130	0.000nm	0.000nm	0.000µm	0.000µm	0.000nm

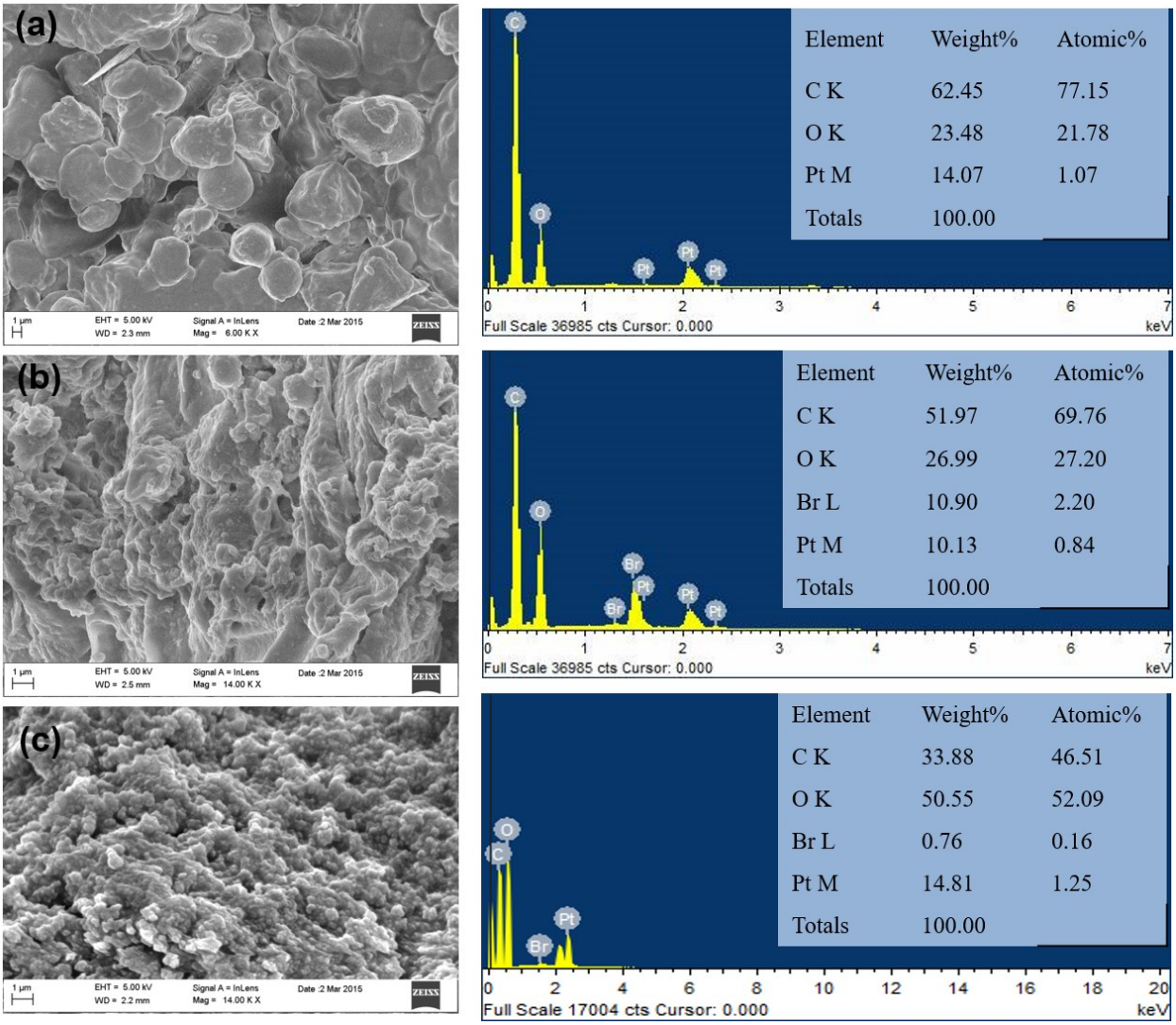

Fig. S5. FESEM and EDAX analysis of (a) TKP, (b) macro initiator, and (c) g-TKP/pMA-18.

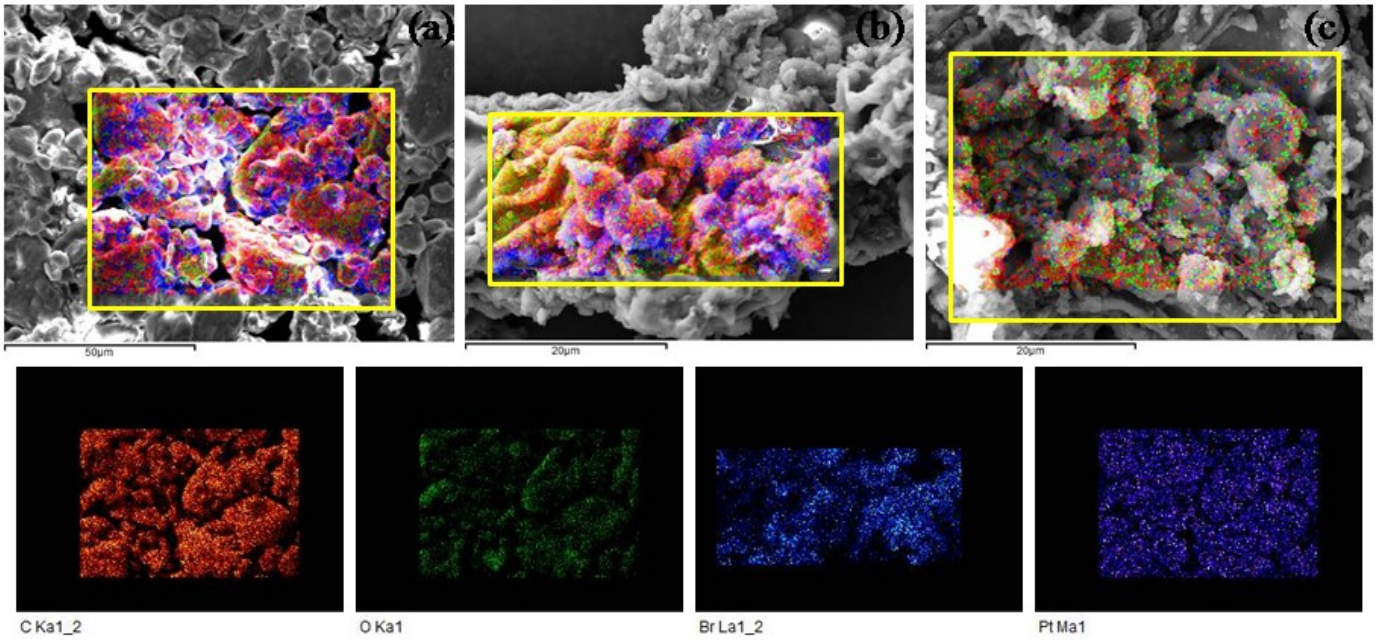

Fig. S6. Elemental mapping of (a) TKP (b) TKP-Br (c) g-TKP/pMA.

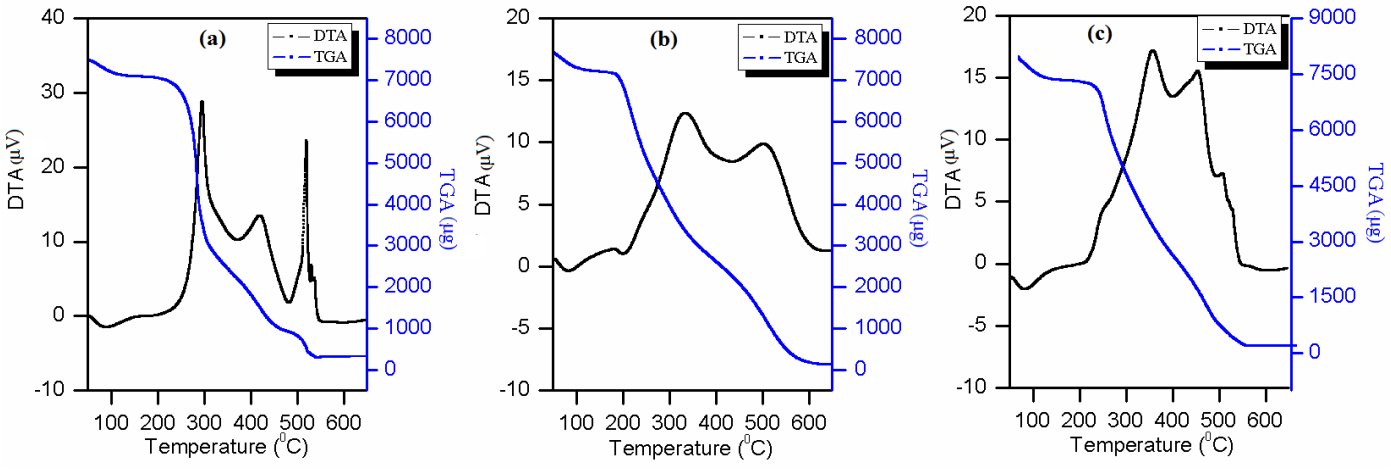

Fig. S7. Thermogravimetric analysis of (a) TKP (B) TKP-Br and (c) g-TKP/pMA

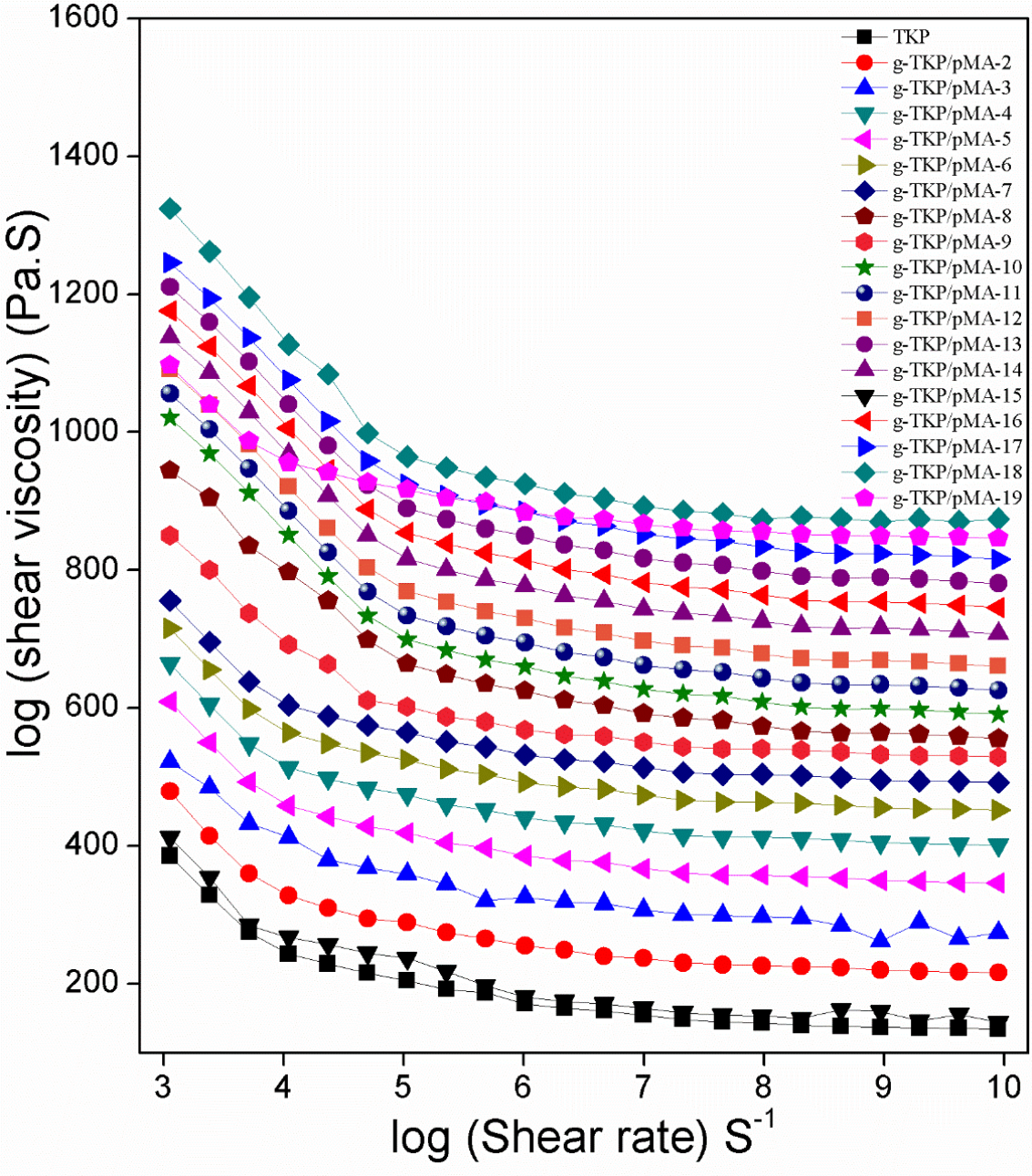

Fig. S8. Shear viscosity vs. shear rate curve of TKP and various g-TKP/pMA.

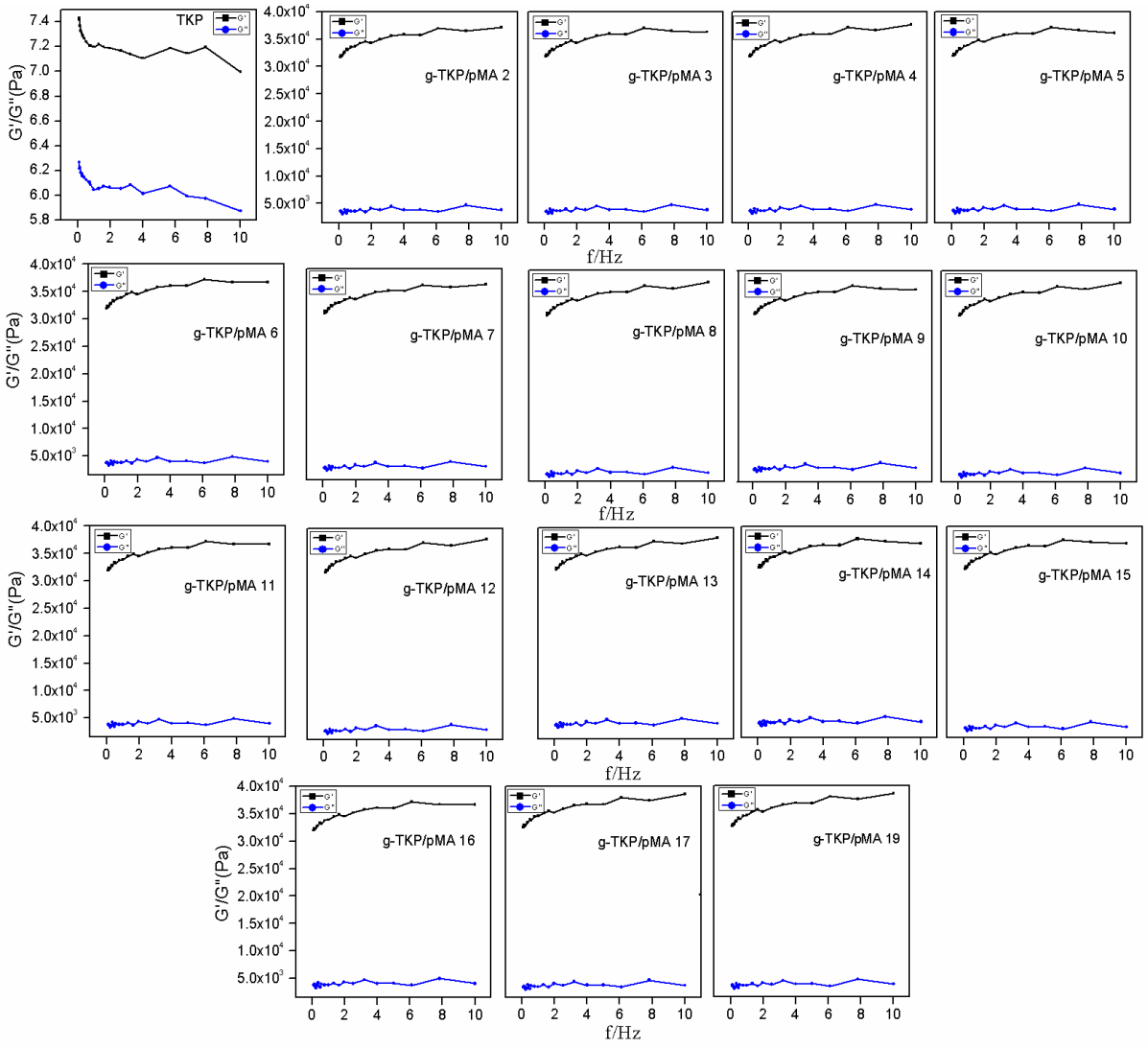

Fig. S9: G′/G″ vs. frequency curve for TKP and various g-TKP/pMA.

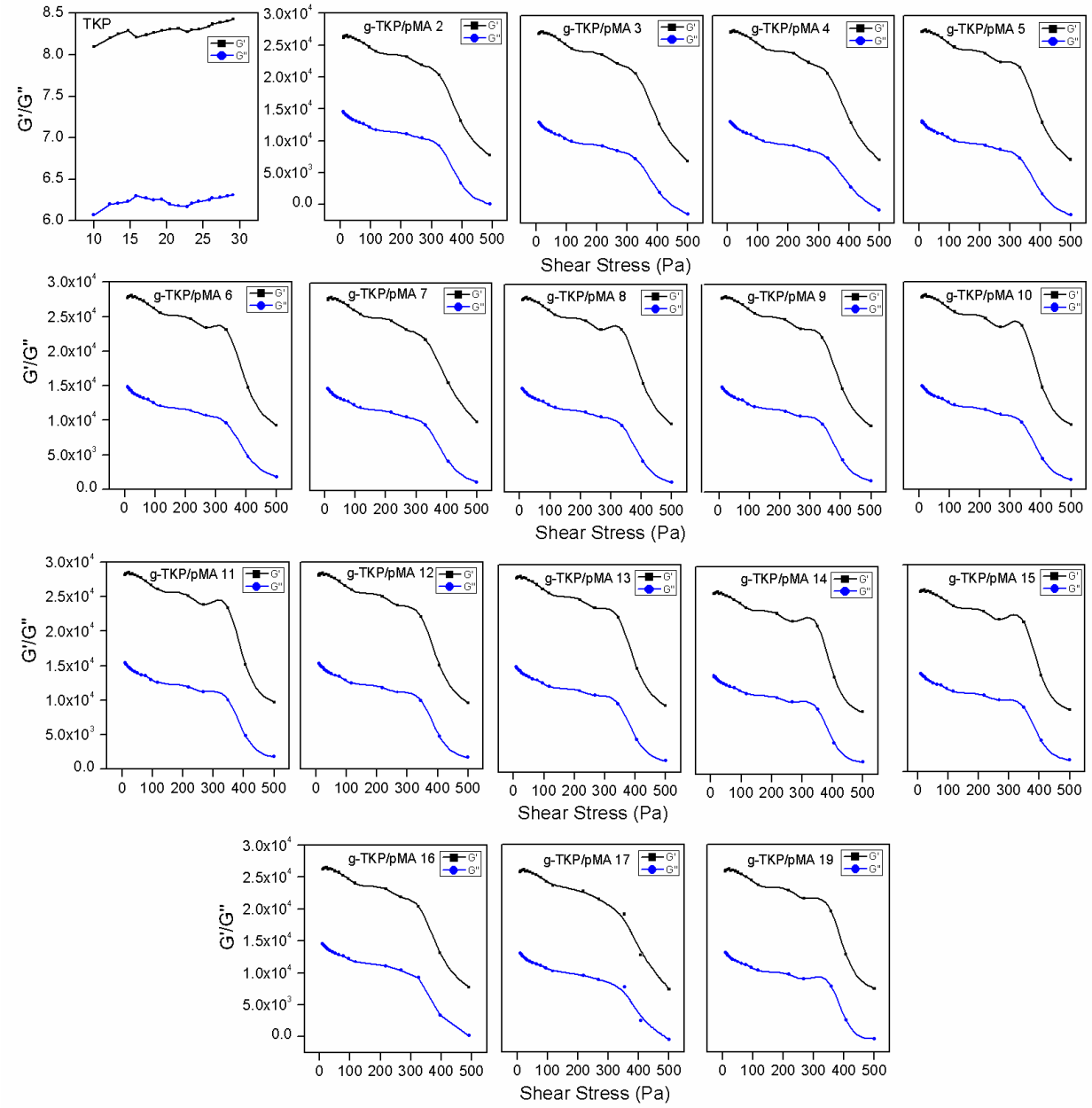

Fig. S10: G′/G″ vs. shear stress curve for TKP and various g-TKP/pMA.

Effect of parameters on % adsorption of dyes:

Effect of dye concentration:

The initial concentration of adsorbate gives a significant driving force to defeat all mass transfer resistances of the dyes between the solid and aqueous phases. Fig. S11a suggests that initially adsorption efficiency was increased upto fixed dosages of dyes concentration, beyond which it was declined. At lower concentrations, all adsorbate ions present in the adsorption medium could react with the binding sites, hence higher % adsorption occurs. At higher concentrations, due to the saturation of the sorption sites, the % uptake of the dyes by the g-TKP/pMA showed a decreasing trend. [1]

Effect of contact time:

Fig. S11b represents that efficiency of the dyes adsorption was increased gradually with time and reached maximum at 25 min (MB), 35 min (Safranin), 30 min (EBT), and 35 min (MO) respectively. This is due to the accessibility of a large number of adsorption sites.[2] Initially the dyes are adsorbed on the surface of adsorbent through Vander Waal's force of attraction followed by the electrostatic attraction or sharing of lone pair of electrons between the adsorbent and adsorbate molecules.[2]After maximum removal, the rate of dyes uptake was controlled by the rate of dyes transport from external to internal pores of the graft copolymer. [2]

Effect of polymer dosage:

The effect of g-TKP/pMA dosage on uptake of dyes from aqueous solution (Fig. S11c) displays that maximum removal took place at 45mg/25 mL for MB and Safranin and 50 mg/25 mL for EBT and MO. This is due to the higher availability of adsorption sites on adsorbent surface, which creates the overcrowding of adsorption sites.[1]

Effect of temperature:

With increase in temperature from 25 ºC to 35 ºC for MB and Safranin, the Adsorption capacity gradually increased and it goes upto 99.07 % and 96.34 %, but 97.67 % and 89.45 % for EBT and MO at 40°C respectively (Fig. S11d) and beyond this it was declined. This is mainly due to the swelling effect of the synthesized polymer which enhanced the adsorption efficiency.[3] Also with the increase in temperature, the mobility of dyes molecules were increased which provides sufficient driving force to overcome mass transfer resistance of the dyes ions between aqueous and surface phase of the polymer.[4] But after certain temperature, the Adsorption efficiency was decreased, due to weakening of adsorption forces between the active sites of the polymer and dyes and also between the adjacent molecules of the adsorbed phase.[5]

Effect of agitation speed:

The effect of agitation speed on adsorption performance of dyes using g-TKP/pMA-18 has been studied and found that the highest adsorption was occurred at 100 rpm (MB, Safranin and MO) and 120 (EBT). Initially with increase in agitation speed, the diffusion rate of the dyes became higher because of the enhancement of turbulence, resulting higher adsorption efficacy and after the certain speed, desorption may predominant owing to the reverse effect [2] (Fig. S11e).

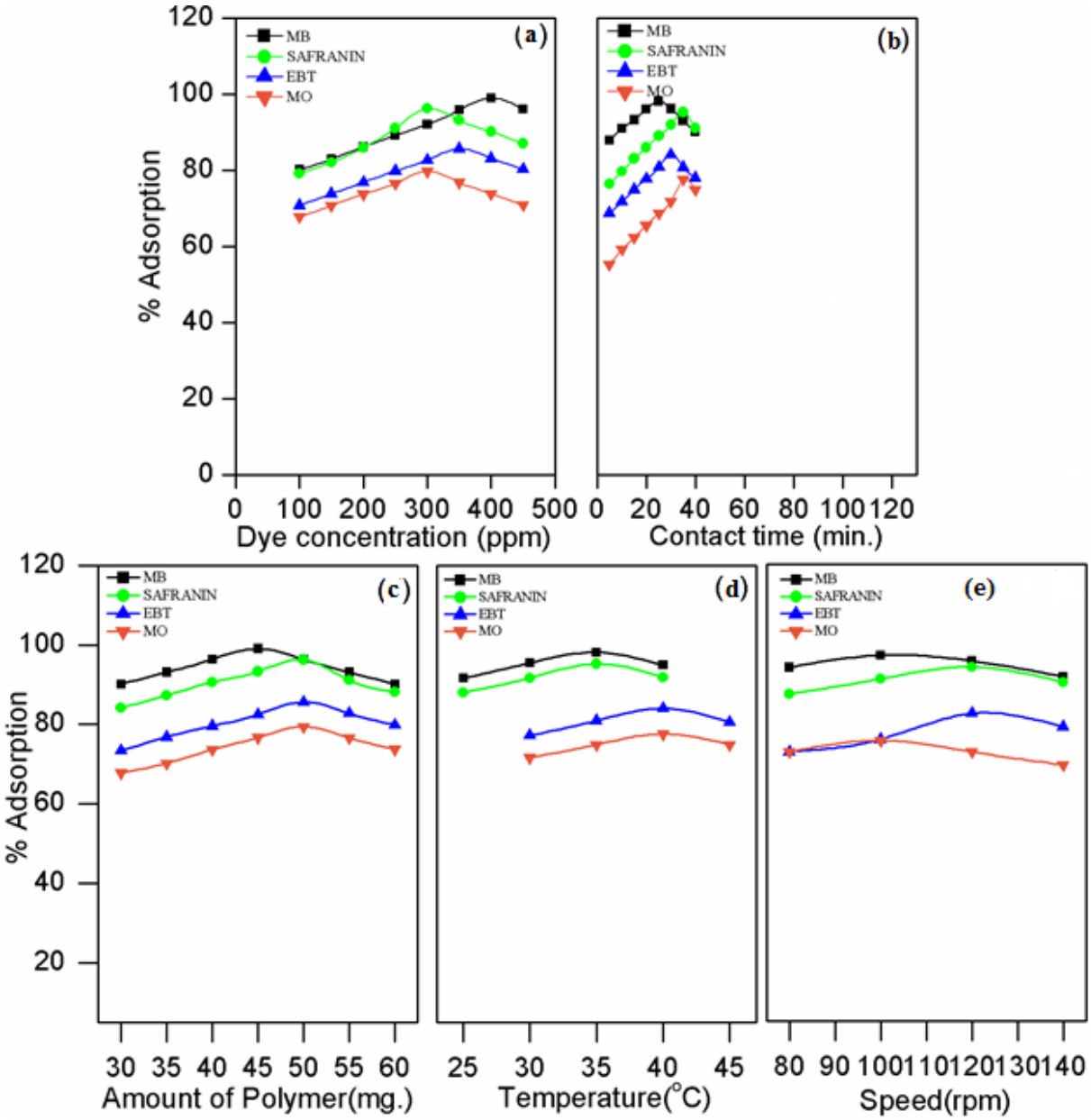

Fig. S11: Effect of (a) dye concentration (b) time, (c) polymer dosage, (d) temperature, (e) speed on % adsorption of various dyes.

Adsorption Kinetics:

The kinetic mechanism was determined using pseudo-first-order, pseudo-second-order and second order models.

The linear form of the pseudo-first order kinetics model is [6]

$$log(q_e - q_t) = logq_e - \frac{K_1}{2.303}t \ldots\ldots\ldots\ldots\ldots\ldots\ldots\ldots\ldots\ldots\ldots (1)$$

Where q_e and q_t (mg/g) refer to the amount of dyes adsorbed at equilibrium and time t (min), respectively, k_1 (min-1) is the rate constant. Fig. S12e-h shows the $log(q_e - q_t)$ vs. *t* plot for the pseudo-first order and the parameters k_1, q_e and the correlation coefficient (R^2) are reported in Table S3.

The second model is pseudo-second order [7]

$$\frac{t}{q_t} = \frac{1}{K_2 q_e^2} + \frac{t}{q_t} \ldots\ldots\ldots\ldots\ldots\ldots\ldots\ldots\ldots\ldots\ldots\ldots (2)$$

Where k_2 is the pseudo-second order rate constant (g mg^{-1} min^{-1}). Fig. S12 a-d represents the t/q_t vs. *t* plot for pseudo-second order and the parameters k_2, q_e and R^2 values are listed in Table S3.

The third model is the second-order rate equation and is represented as [8]

$$\frac{1}{(q_e - q_t)} = \frac{1}{q_e} + K_3 t \ldots\ldots\ldots\ldots\ldots\ldots\ldots\ldots\ldots\ldots\ldots\ldots (3)$$

Where k_3 is the second order rate constant (g mg^{-1} min^{-1}), Fig. S12 (i-l) shows $1/(q_e - q_t)$ vs. *t* plot for the second order and the parameters k_3, q_e and R^2 are listed in Table S3.

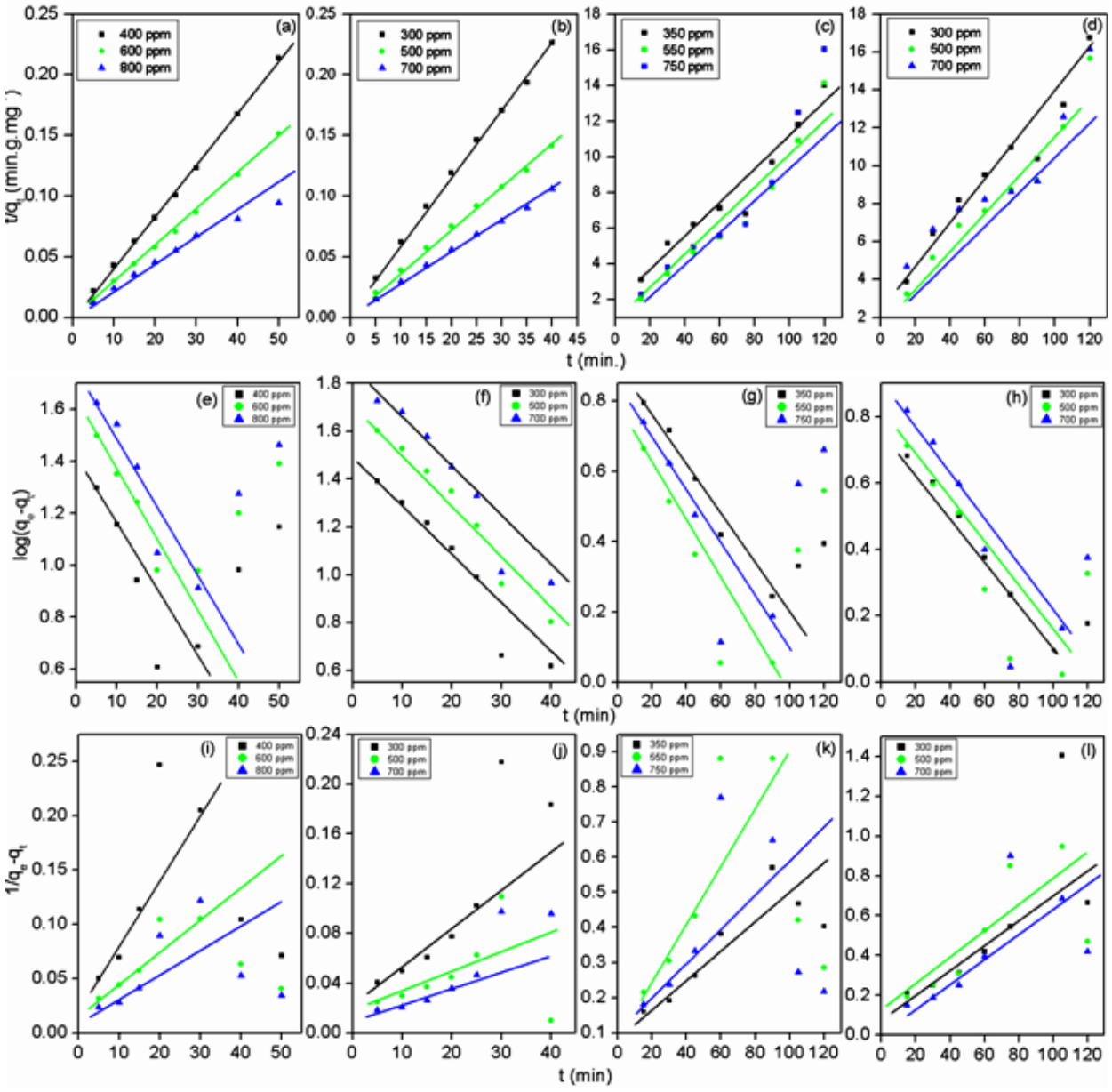

Fig. S12: Kinetics modeling of pseudo-second order model of (a) MB, (b) Safranin, (c) EBT, (d) MO, Pseudo-first order model of (e) MB, (f) Safranin, (g) EBT, (h) MO and second order model of (i) MB, (j) Safranin, (k) EBT, (l) MO using g-TKP/pMA-18adsorbent.

Table S3. Kinetics parameters for adsorption of various dyes using g-TKP/pMA adsorbent

Dye	Conc.	Pseudo -first order			Pseudo-second order			Second order		
	(ppm)	K_1 (min^{-1})	q_e ($mg.g^{-1}$)	R^2	K_2 ($g.mg^{-1}min^{-1}$)	q_e ($mg.g^{-1}$)	R^2	K_3 ($g.mg^{-1}min^{-1}$)	q_e ($mg.g^{-1}$)	R^2
	400	0.0057	50.856	0.6238	0.0133	235.84	0.9983	0.0034	28.71	0.4936
MB	600	0.0053	59.579	0.5654	0.0081	334.44	0.9977	0.0025	37.39	04738
	800	0.0045	62.584	0.5387	0.0078	442.90	0.9967	0.0019	45.90	0.4627
	300	0.0561	45.253	0.5625	0.0037	183.82	0.9982	0.0058	35.72	0.3163
SF	500	0.0559	52.261	0.4815	0.0022	294.11	0.9970	0.0054	42.31	0.2798
	700	0.0549	60.326	0.4381	0.0016	393.70	0.9958	0.0051	48.85	0.2231
	350	0.0004	46.271	0.4842	0.0057	210.34	0.9273	0.0031	23.24	0.4371
EBT	550	0.0039	57.453	0.4564	0.0042	261.35	0.9228	0.0016	30.17	0.4250
	750	0.0024	62.432	0.4324	0.0028	274.41	0.8794	0.0007	41.04	0.3998
	300	0.0152	35.563	0.4106	0.0038	192.55	0.9070	0.0082	25.84	0.3373
MO	500	0.0131	37.453	0.3738	0.0032	199.77	0.8951	0.0053	27.32	0.3202
	700	0.0121	39.864	0.3675	0.0027	210.96	0.8474	0.0045	31.30	0.2972

Adsorption isotherm:

The linear form of Langmuir isotherm is given by the following equation[9]

$$\frac{C_e}{q_e} = \frac{1}{b.Q_0} + \frac{C_e}{Q_0} \quad ----------(4)$$

Where C_e is the equilibrium concentration of adsorbate ($mg.L^{-1}$), q_e is the amount of dyes adsorbed by the adsorbent at equilibrium (mg.g-1), the Langmuir constant Q_0 ($mg.\ g^{-1}$) represents the monolayer adsorption capacity and b ($L.mg^{-1}$) represents the heat of adsorption. Fig. S13a-d shows the linear plot C_e/q_e against C_e for Langmuir isotherm and the parameters Q_0, b and R^2 are listed in Table S4.

The feasibility of the adsorption process is determined using separation factor (R_L), which is defined by following equation[10]

$$R_L = \frac{1}{1 + bC_0} \quad ----------(5)$$

Where b = Langmuir constant and C_0= initial concentration of various dyes. The value of R_L indicates the category of the isotherm to be either unfavorable (R_L>1), linear (R_L=1), irreversible (R_L=0) or favorable (0<R_L<1).

The Freundlich isotherm is given by the following equation[11]

$$q_e = K_f.C_e^{1/n} \quad ----------(6)$$

Where K_f ($mg.g^{-1}$) and n are Freundlich constants related to the capacity and favorability of sorption respectively. Fig. S13e-h represents the linear plots of $ln\ q_e$ vs. $ln\ C_e$ for Freundlich isotherm and the parameters n, K_f and R^2 are listed in Table S4. It is noted that greater is the n value, better is the favorability of the adsorption and the monolayer adsorption capacity (Q_{max}) of

g-TKP/pMA was found to be extremely high for MB (571.42mg/g) at 308K. It has also been shown that the R_L (separation factor) [12] values is in between 0 to 1, which signifies that the adsorption process is favorable. Also, with increase in temperature, the Langmuir constant (b) was found to be increased (Table S4) which indicates the stronger attraction between the active sites of the adsorbent and adsorbate as well as the higher affinity of adsorbent and adsorbate molecules at higher temperature in contrast to lower temperature.[10]

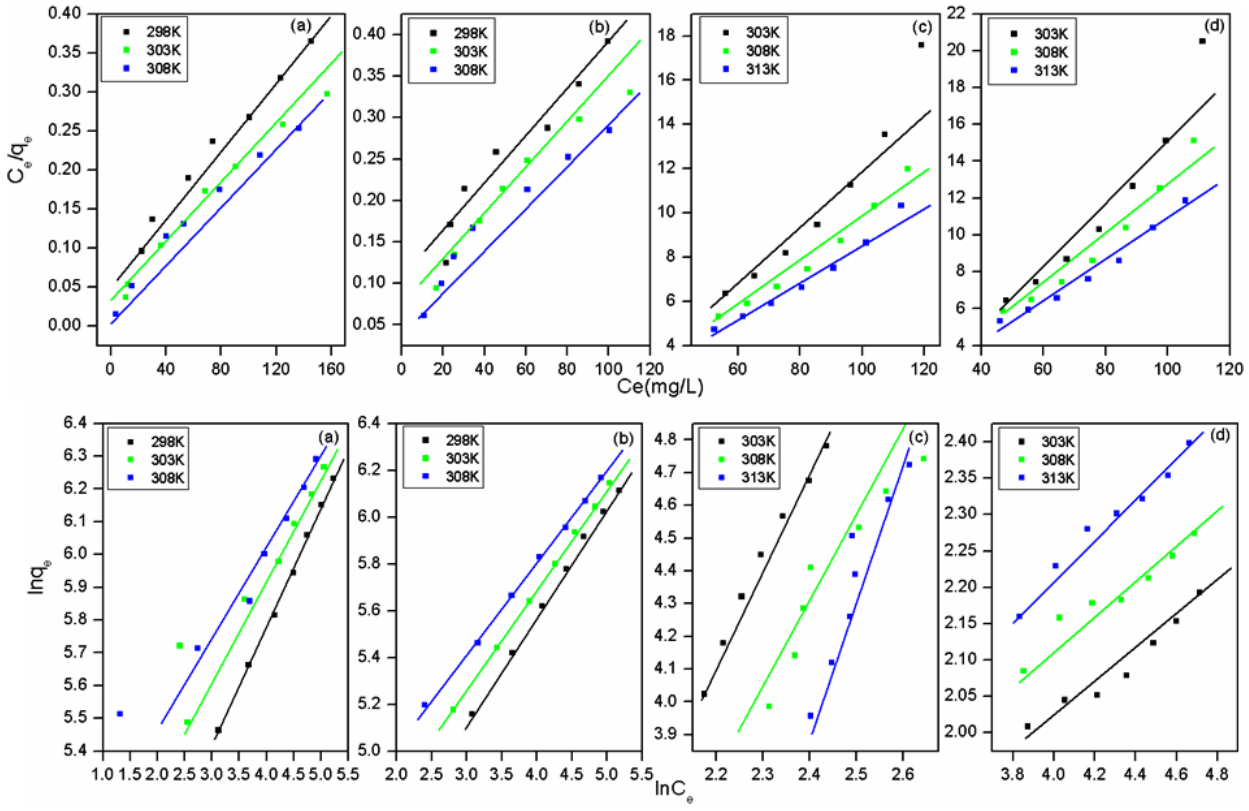

Fig. S13: Langmuir isotherm model for (a) MB, (b) Safranin, (c) EBT and (d) MO and Freundlich isotherm model for (e) MB, (f) Safranin, (g) EBT and (h) MO using g-TKP/pMA

Table S4: Parameters for Langmuir and Freundlich isotherm for various dyes adsorption.

Dyes	Temp. (K)	Langmuir model			Freundlich model		
		Q_{max} (mg.g-1)	b (L.mg-1)	R^2	K_f(mg.g-1)	n	R^2
	298K	485.43	0.0307	0.9841	74.48	2.72	0.8977
MB	303K	568.18	0.0410	0.9862	146.68	4.06	0.9456
	308K	571.42	0.0628	0.9932	175.38	4.64	0.9754
	298K	347.22	0.0288	0.9634	42.09	2.16	0.8734
SF	303K	400.00	0.0330	0.9734	51.80	2.95	0.9280
	308K	421.94	0.0389	0.9837	70.63	2.98	0.9473
	303K	435.47	0.0407	0.9309	57.92	2.75	0.8290
EBT	308K	467.89	0.0860	0.9692	79.88	2.85	0.8637
	313K	481.34	0.1255	0.9796	81.23	2.97	0.8941
	303K	270.67	0.0423	0.9229	43.82	2.56	0.7823
MO	308K	298.89	0.0795	0.9569	54.71	2.64	0.8336
	313K	373.67	0.1191	0.9710	65.03	2.77	0.8577

Adsorption Thermodynamics:

The feasibility and spontaneity of the dyes uptake have been discussed using Van't Hoff's equation:

$$lnb = \frac{\Delta S^o}{R} - \frac{\Delta H^o}{RT} - - - - - - - - - - - - (7)$$

$$\Delta G^o = \Delta H^o - T\Delta S^o - - - - - - - - - - (8)$$

Where ΔG^o is the change in Gibbs free energy (J. mol^{-1}), ΔH^o is change in enthalpy (J. mol^{-1}), ΔS^o is the change in entropy (J. mol^{-1} K^{-1}), R is universal gas constant (8.314 J. K^{-1} mol^{-1}) and b is Langmuir constant at temperature T (K). Fig. S14a-d represents the plot of $ln\ b$vs.$1/T$ and thermodynamics parameters like ΔG^o, ΔH^o and ΔS^o has been reported in Table S5.

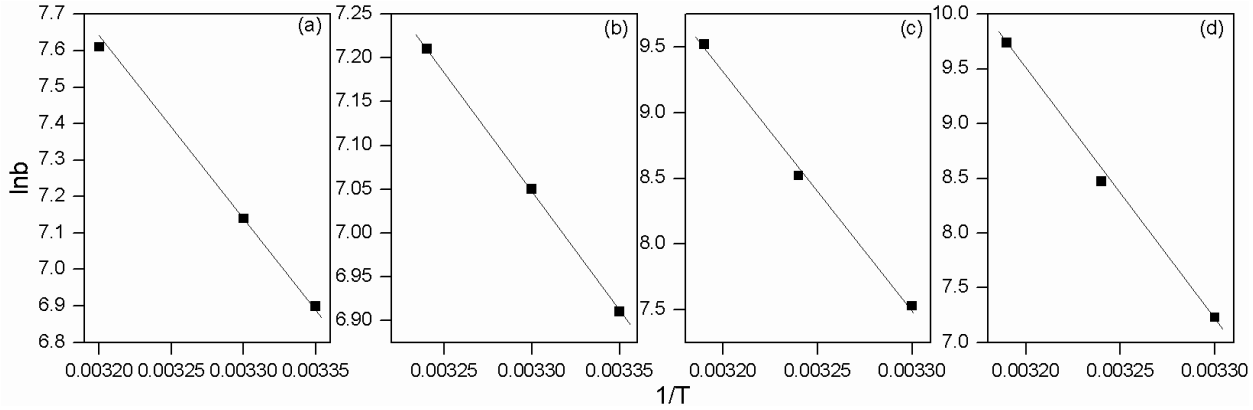

Fig. S14: ln b vs. 1/T plot for (a) MB (b) Safranin, (c) EBT, (d) MO, using g-TKP/pMA-18 adsorbent.

Table S5: Thermodynamic parameters for uptake of various dyes using g-TKP/pMA

Dye	Temp. (K)	Δ Gº (KJ mol-1)	Δ Hº (KJ mol-1)	ΔSº (KJ mol-1K-1)
	298K	-33.538		
MB	303K	-34.480	22.698	0.1887
	308K	-35.424		
	298K	-17.066		
SF	303K	-17.732	22.657	0.1333
	308K	-18.399		
	303K	-25.758		
EBT	308K	-26.463	14.983	0.1410
	313K	-27.168		
	303K	-15.050		
MO	308K	-15.609	18.825	0.1118
	313K	-17.895		

Desorption study:

The graft copolymer (g-TKP/pMA) shows excellent regeneration characteristics, which reduce the overall cost of the adsorbent. Maximum % desorption was obtained in acidic medium for cationic dyes (pH 2: 96.89 % for MB, 94.12 % for Safranin) and basic medium for anionic dyes (pH 9: 95.34 % for EBT and 86.34 % for MO). Besides, the minimum % of desorption was observed at basic condition for MB and Safranin dyes (pH 9: 40.47% for MB, 38.32% for Safranin) and that of 37.56 % for EBT and 32.37% for MO at acidic environment. The dye desorption process follows ion exchange mechanism [12, 13] which has been depicted in Fig. S15.

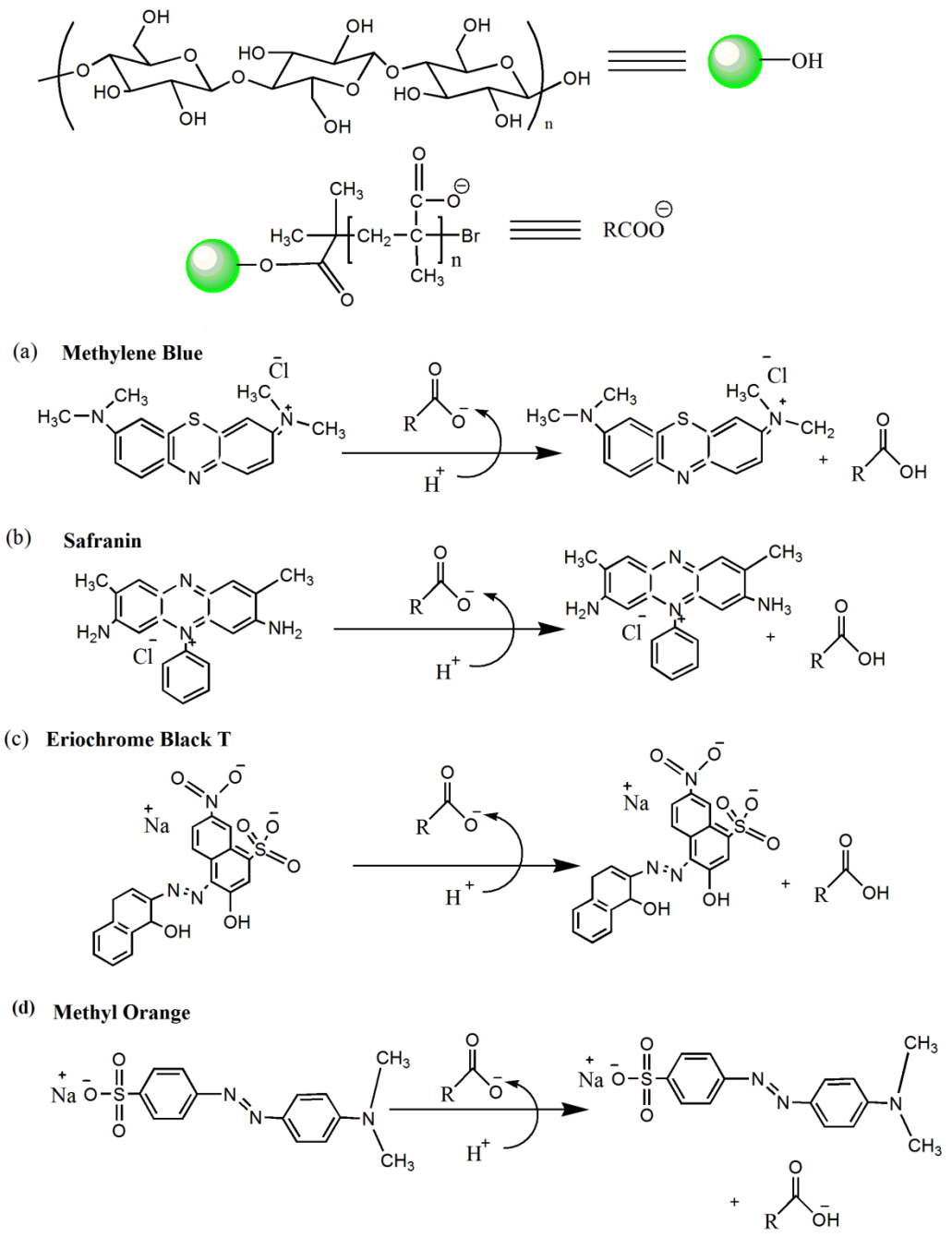

Fig. S15: Desorption mechanism of (a) MB (b) SF (c) EBT and (d) MO dyes.

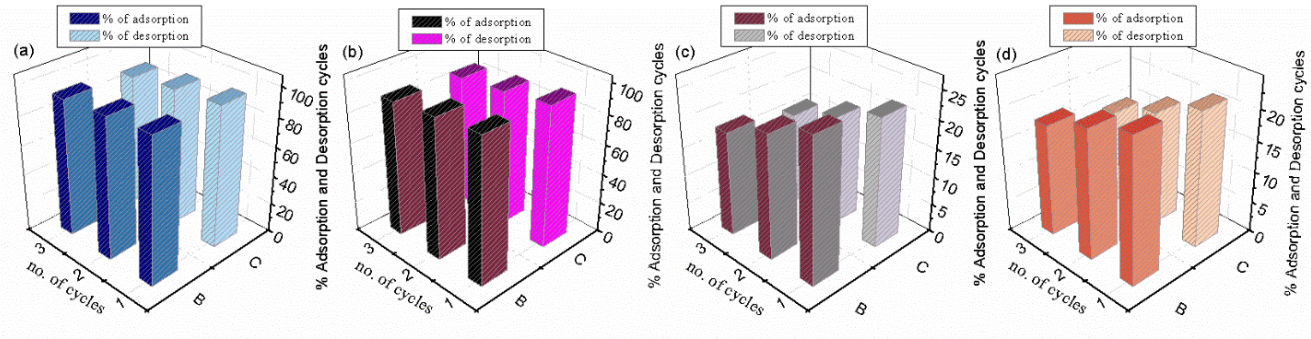

Fig. S16: Adsorption-desorption cycles of (a) MB (b) SF (c) EBT and (d) MO dyes.

Table S6. Comparison of maximum adsorption capacity of g-TKP/pMA with other reported adsorbents for removal of MB and EBT dye from aqueous environment.

Adsorbent	Adsorption capacity for removal of MB (Q_{max}) (mg. g^{-1})	Reference	Adsorbent	Adsorption capacity for removal of EBT (Q_{max}) (mg. g^{-1})	Reference
Polyaniline NanotubesBase	8.21	[10]	Activated carbon	160.36	[24]
Activated carbon coated palygorskite	351	[14]	eucalyptus bark	136.7	[25]
pyrolytic tire char	65.81	[15]	$NiFe_2O_4$ magnetic Nanoparticles	47.0	[26]
Diatomite treated with sodium hydroxide	27.86	[16]	Modified Kaolin Clay and Talc	109.0	[27]
Boron-doped diamond (BDD) electrode	33.57	[17]	Activated Nilgiri leaves	33.33	[28]
Nitric acid modification of activated carbon	480.4	[18]	MnO_2-Coated Zeolite	12.35	[29]
Natural palygorskite modification by introducing sodium silicate and magnesium salts	527.22	[19]	Bentonite Carbon Composite Material	11.51	[30]
γ-Al2O3 nano-structured hierarchical hollowmicrospheres	8.38	[20]	Modification of Activated Carbon	158.73	[31]
Dodecyl sulfobetaine surfactant-modified montmorillonite	254.0	[21]	Bioaugmented Aerobic Granules	200	[32]
Polydopamine microspheres	90.7	[22]	Scolymus Hispanicus L.	165.77	[32]
Modified natural palygorskite	158.03	[23]	**g-TKP/pMA-18**	481.34	**Present study**
g-TKP/pMA-18	571.42	**Present study**			

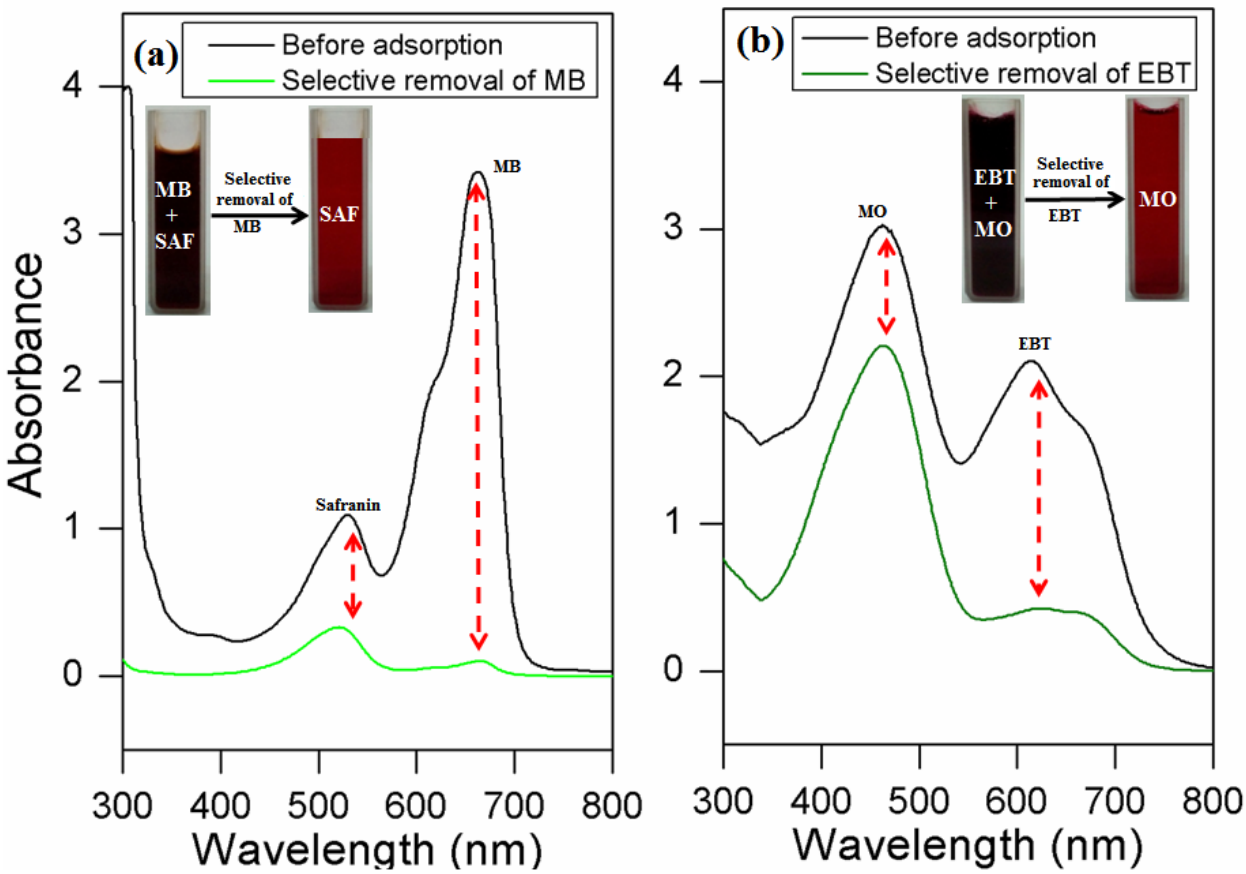

Fig. S17: UV-Vis spectra of mixed (a) cationic and (b) anionic dyes solution before and after adsorption treatment.

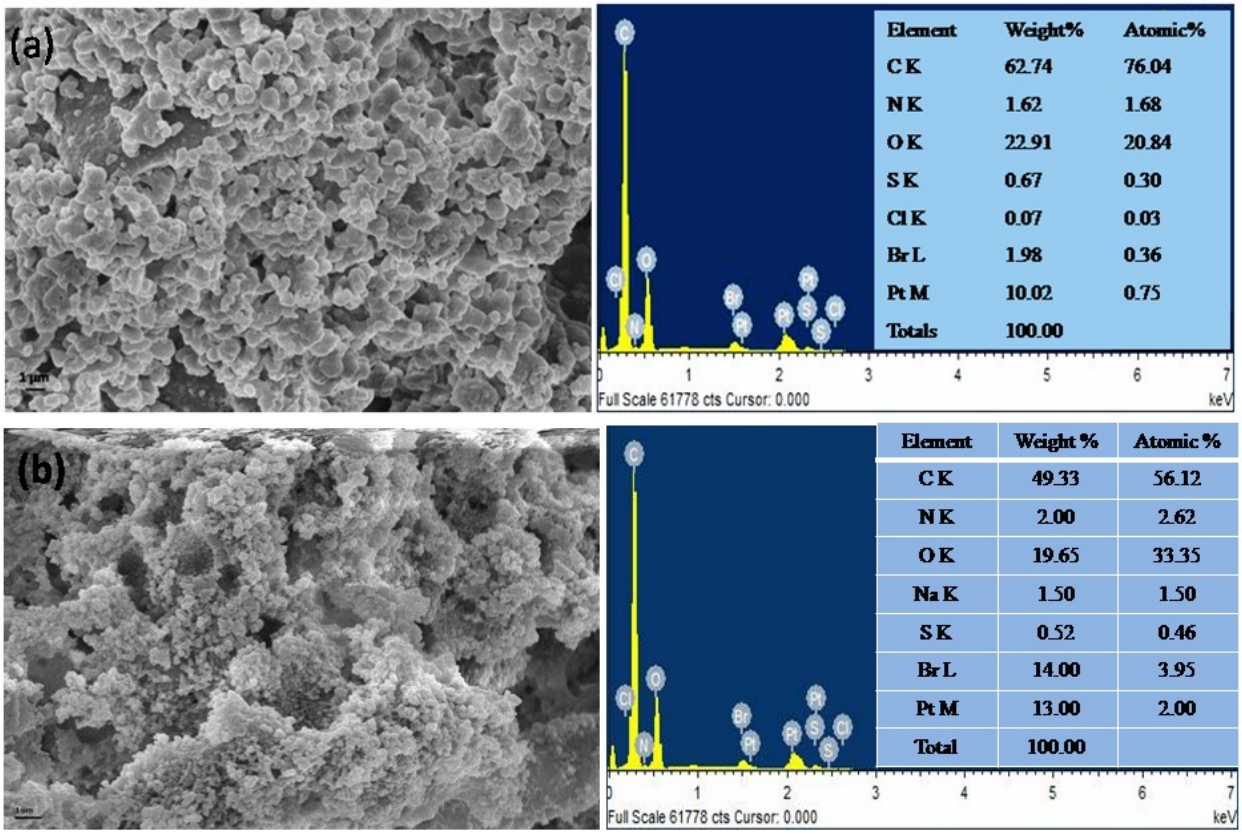

Fig. S18: FESEM and EDAX of g-TKP/pMA-18 loaded (a) MB and (b) EBT.

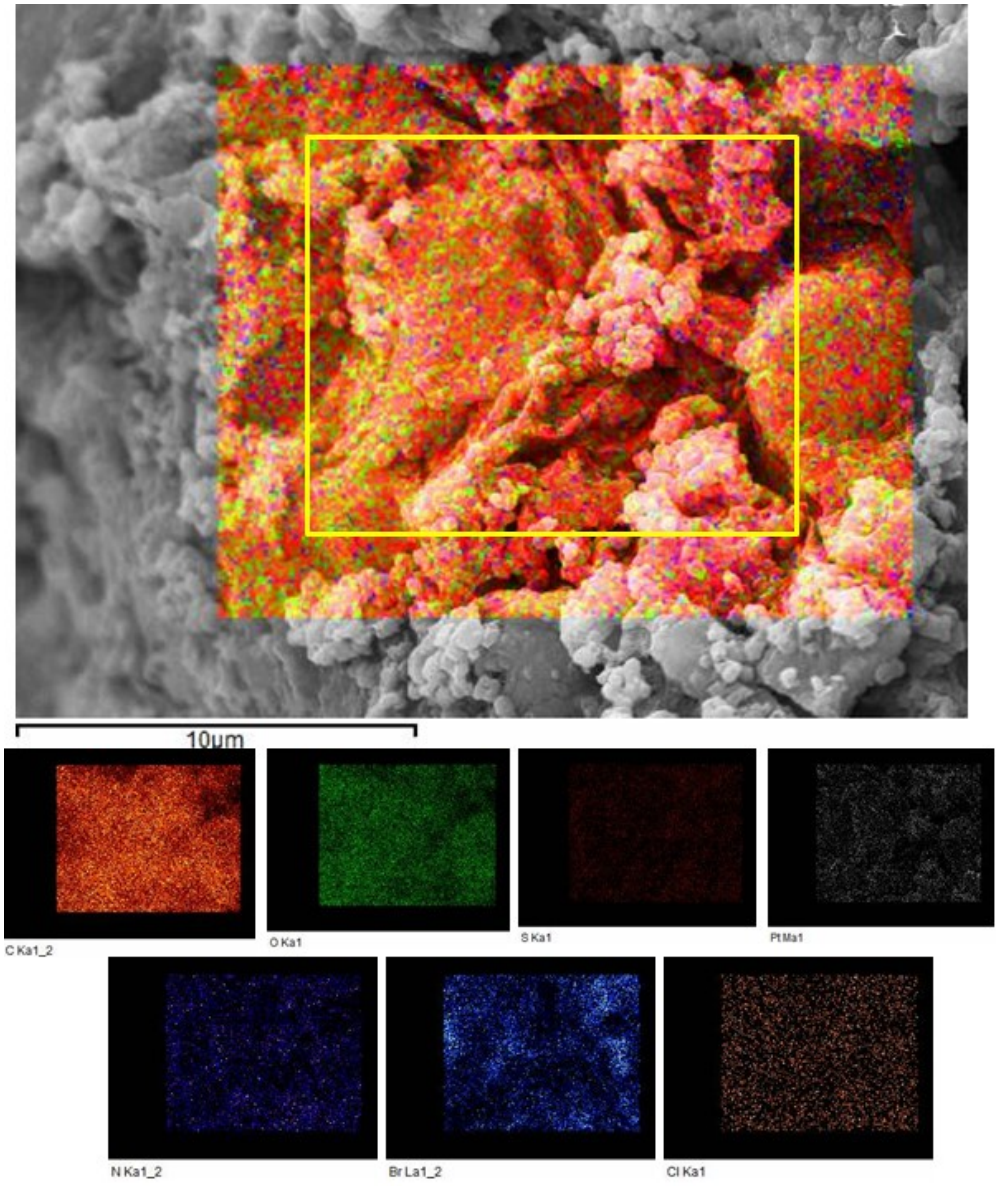

Fig. S19: Elemental mapping of g-TKP/pMA-18 loaded MB dye.

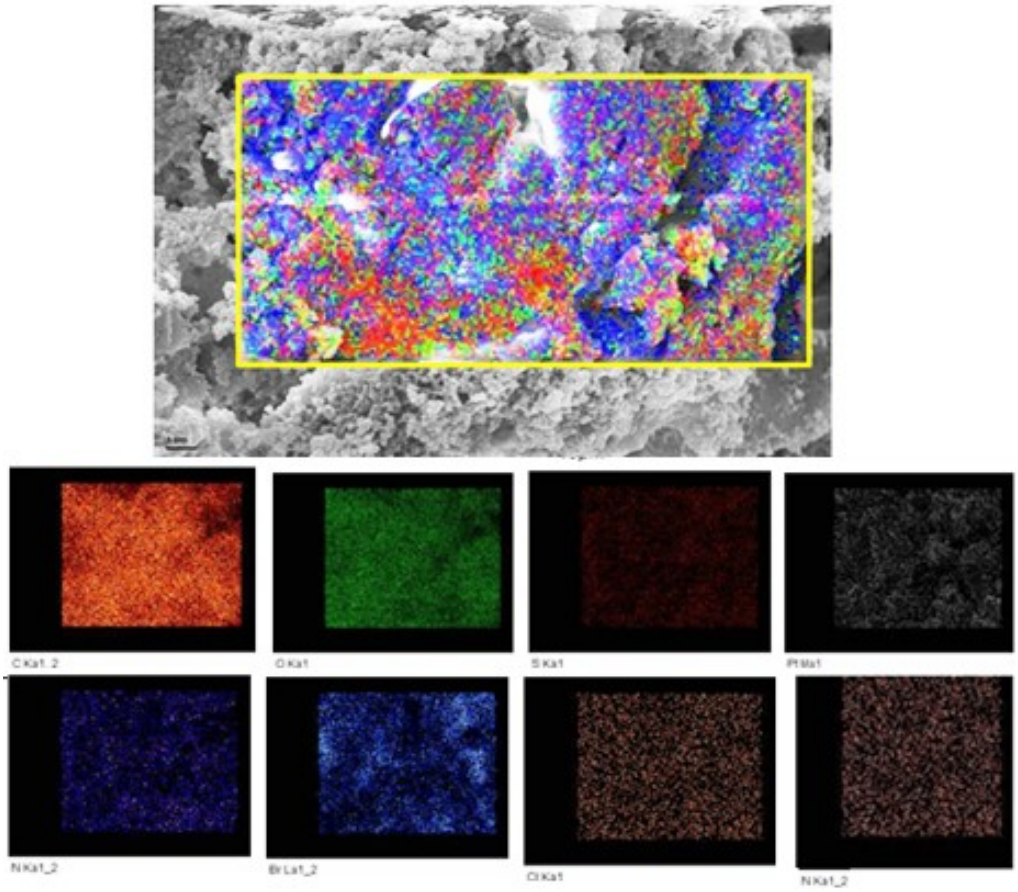

Fig. S20: Elemental mapping of g-TKP/pMA-18 loaded EBT.

Table S7: Characteristics FTIR spectra peaks of g-TKP/pMA-18, MB and EBT adsorbed g-TKP/pMA-18

Characteristics peaks	g-TKP/pMA(cm^{-1})	MB adsorbed g-TKP/pMA(cm^{-1})	EBT adsorbed g-TKP/pMA(cm^{-1})
–OH stretching	3418	3389	3408
C−H stretching	2926	2923	2921
COO^- asymmetric stretching	1538	1530	1518
COO^- symmetric stretching	1458	1438	1432
-OH bending vibration	1388	1378	1376
C-Br stretching	625	614	603

References:

(1) K. K. Singh, M. Talat and S. H. Hasan, *Bioresour. Technol.,* 2006, **97**, 2124–2130.

(2) S. Ghorai, A. K. Sarkar and S. Pal, *Bioresour. Technol.* 2014, **170**, 578–582.

(3) L. Wang, J. Zhang and A. Wang, *Desalination,* 2011, **266***,* 33–39.

(4) D. Lua, Q. Cao, X. Cao and F. Luo, *J. Hazard. Mater*., 2009, **166**, 239–247.

(5) V. K. Gupta and Suhas, *J. Environ. Manage.*, 2009, **90**, 2313–2342.

(6) S. Legergren, *K. SvenskaVetenskapsakad. Handl.*, 1898, **24**, 1−39.

(7) Y. S. Ho and G. McKay, *Process Biochem.*, 1999, **34**, 451–465.

(8) Y. S. Ho, *Water Res*., 2006, **40***,* 119 – 125.

(9) I. Langmuir, *J. Am.Chem. Soc.*, 1916, **38**, 2221−2295.

(10) M. M. Ayad and A. A. El-Nasr, *J. Phys. Chem. C* 2010, **114**, 14377–14383.

(11) H. M. F. Freundlich, *Z. Phys. Chem.*, 1906, **57**, 385−470.

(12) A. Pal, D. Das, A. K. Sarkar, S. Ghorai, R. Das and S. Pal, *Eur. Polym. J.*, 2015, **66**, 33–46.

(13) A. Heidaria, H. Younesia, Z. Mehrabanb and H. Heikkinen, *Int. J. Biol. Macromol*., 2013, **61**, 251– 263.

(14) X. Zhang, L. Cheng, X. Wu, Y. Tang and Y. Wu, *J. Environ. Sci.*, 2015, **33**, 97-105.

(15) V. Makrigianni, A. Giannakas, Y. Deligiannakis and I. Konstantinou, *J. Environ. Chem. Eng.*, 2015, **3**, 574–582.

(16) Z. Jian, P.Qingwei, N. Meihong, S. Haiqiang and L. Na, *Appl. Clay Sci.,* 2013, **83–84**, 12 -16.

(17) H. Akrout, S. Jellali and L. Bousselmi, *C. R. Chimie.*, 2015**, 18**, 110–120.

(18) Y. Gokce and Z. Aktas, *Appl. Sur. Sci.*, 2014, **313**, 352–359.

(19) W. Wanga, G. Tian, Z. Zhang, A. Wang, *Chem. Eng. J.*, 2015, **265**, 228–238.

(20) J. Fang, X. Huang, X. Ouyang and X. Wang, *Chem. Eng. J.*, 2015, **270**, 309–319.

(21) H. Fan, L. Zhou, X. Jiang, Q. Huang and W. Lang, *Appl. Clay Sci.*, 2014, **95**, 150–158.

(22) J. Fu, Z. Chen, M. Wanga, S. Liu, J. Zhang, J. Zhang, R. Han and Q. Xu, *Chem. Eng. J.*, 2015, **259**, 53–61.

(23) Y. Zhang, W. Wang, J. Zhang, P. Liu and A. Wang, *Chem. Eng. J.*, 2015, **262**, 390–398.

(24) M. Daniel, G. D. Luna, E. D. Floresb, D. Angela, D. Genuino, C. M. Futalan and M. W. Wan, *J. Taiwan Inst. Chem. Eng.*, 2013**, 44**, 646–653.

(25) P. N. Davea, S. Kaurb and E. Khosla, *Ind. J. Chem. Technol*., 2011, **18**, 53-60.

(26) F. Moeinpour, A. Alimoradi and M. Kazemi, *J. Environ. Health Sci. Eng.*, 2014, **12**, 112.

(27) H. J. Sonba and S. H. Ridha, *Acta Chim. Pharm. Indica.*, 2014, **4**, 111-118.

(28) U. V. Ladhe, S. K. Wankhede, V. T. Patil and P. R. Patil, *J. Chem. Pharm. Res*., 2011, **3**, 670-675.

(29) D. Marie, M. Aguila and M. V. Ligaray, *Inter. J. Environ. Sci. Dev.*, 2015, **6**, 824-827.

(30) F. M. S. E. El-Dars, H. M. Ibrahim, H. A. Farag, M. Z. BAbdelwahhab and M. E. H. Shalabi, *Inter. J. Sci. Eng. Res*., 2015, **6**, 679-688.

(31) E. Alzahrani, *Inter. J. Recent Technol. Eng*., 2014, **3**, 6-10.

(32) W. Hailei, L. Pinga, L. Guoshenga, L. Xina, Y. Jianming, *Enzyme Microb. Tech*., 2010, **47**, 37–43.